The Astrophysical Journal, 805:179 (9pp), 2015 June 1 doi:10.1088/0004-637X/805/2/179

THE EVENT HORIZON OF M87

Avery E. Broderick[1,2], Ramesh Narayan[3], John Kormendy[4,5,6], Eric S. Perlman[7], Marcia J. Rieke[8], and Sheperd S. Doeleman[3,9]
[1] Perimeter Institute for Theoretical Physics, 31 Caroline Street North, Waterloo, ON, N2L 2Y5, Canada
[2] Department of Physics and Astronomy, University of Waterloo, 200 University Avenue West, Waterloo, ON, N2L 3G1, Canada
[3] Harvard-Smithsonian Center for Astrophysics, 60 Garden Street, Cambridge, MA 02138, USA
[4] Department of Astronomy, University of Texas at Austin, 2515 Speedway, Mail Stop C1400, Austin, TX 78712-1205, USA; kormendy@astro.as.utexas.edu
[5] Max-Planck-Institut für Extraterrestrische Physik, Giessenbachstrasse, D-85748 Garching-bei-München, Germany
[6] Universitäts-Sternwarte, Scheinerstrasse 1, D-81679 München, Germany
[7] Department of Physics and Space Sciences, Florida Institute of Technology, 150 W. University Blvd., Melbourne, FL 32901, USA; eperlman@fit.edu
[8] Steward Observatory, University of Arizona, 933 North Cherry Avenue, Tucson, AZ 85721-006 USA
[9] MIT Haystack Observatory, Off Route 40, Westford, MA 01886, USA
Received 2015 February 27; accepted 2015 April 9; published 2015 June 2

ABSTRACT

The $6 \times 10^9\ M_\odot$ supermassive black hole at the center of the giant elliptical galaxy M87 powers a relativistic jet. Observations at millimeter wavelengths with the Event Horizon Telescope have localized the emission from the base of this jet to angular scales comparable to the putative black hole horizon. The jet might be powered directly by an accretion disk or by electromagnetic extraction of the rotational energy of the black hole. However, even the latter mechanism requires a confining thick accretion disk to maintain the required magnetic flux near the black hole. Therefore, regardless of the jet mechanism, the observed jet power in M87 implies a certain minimum mass accretion rate. If the central compact object in M87 were not a black hole but had a surface, this accretion would result in considerable thermal near-infrared and optical emission from the surface. Current flux limits on the nucleus of M87 strongly constrain any such surface emission. This rules out the presence of a surface and thereby provides indirect evidence for an event horizon.

Key words: black hole physics – galaxies: individual (M87) – gravitation – radio continuum: galaxies – infrared: galaxies – ultraviolet: galaxies

1. INTRODUCTION

It is now widely accepted that active galactic nuclei (AGNs) are powered by supermassive objects (reaching $10^{10}\ M_\odot$) that are sufficiently compact to exclude all other astrophysically credible alternatives to black holes (Rees 1984). However, it is less clear that these objects possess the defining characteristic of a black hole: an event horizon.[10] The existence of black hole event horizons plays a central role in a number of puzzles associated with black holes, e.g., the information paradox. A number of recent results suggest that a resolution of these puzzles may result in modifications on horizon scales (e.g., Mathur 2011; Almheiri et al. 2013; Mathur 2014), which provides strong motivation for seeking astronomical evidence for the reality of event horizons.

Accretion onto compact objects with a surface, e.g., white dwarfs, neutrons stars, results in the formation of a boundary layer in which any remaining kinetic energy contained within the accretion flow is thermalized and radiated. In contrast, gas accreting onto a black hole is free to advect any excess energy across the horizon without further observational consequence. If the mass accretion rate across the horizon, $\dot{M}$, can be independently estimated, this difference provides an observational means to distinguish between the presence of a surface, or more accurately a "photosphere," and a horizon.

The above argument has already been used to argue for the existence of event horizons in X-ray binaries by comparing neutron star and black hole systems in aggregate (Narayan et al. 1997; Garcia et al. 2001; Narayan & Heyl 2002; Done & Gierliński 2003; Narayan & McClintock 2008). However, the advent of horizon-resolving observations, enabled by millimeter-wavelength very long baseline intererometric observations (mm-VLBI) carried out by the Event Horizon Telescope (EHT, Doeleman et al. 2008, 2009; Doeleman 2010; Fish et al. 2011; Doeleman et al. 2012), has made it possible to extended the argument to individual systems. This is primarily because restricting the size of any photospheric emission to horizon scales enables two important simplifications.

1. Any putative photosphere that lies within the photon orbit is expected to radiate to a good approximation like a blackbody, independently of the details of its composition (Broderick & Narayan 2006, 2007). This is because a majority of the photons emitted from the photosphere will be strongly lensed back onto the photosphere, thermally coupling the photosphere to itself and to the emitted photon field. As the redshift of the surface increases, the blackbody approximation becomes increasingly accurate.
2. The expected temperature of the photosphere emission, as seen by distant observers, is dependent upon the mass accretion rate $\dot{M}$ and the apparent photosphere size, the latter of which is fixed when the photosphere lies within the photon orbit. Thus, assuming that the system has reached steady state,[11] any independent estimate of $\dot{M}$

[10] Here we will employ an astrophysically motivated definition of the horizon: a surface from inside which astronomical signals cannot propagate to large distances in astronomically relevant timescales. Formally, for a dynamical system, such a surface is identified with the apparent horizon. However, in the context of astrophysical black holes described by general relativity, it corresponds to the event horizon as well.

[11] The additional gravitational time delay for radiation to escape from a compact surface is insufficient to prevent the system from reaching steady state, since the timescale diverges only logarithmically as the radius of the surface approaches the horizon radius (Broderick & Narayan 2006; Narayan & McClintock 2008; Broderick et al. 2009).

immediately determines both the luminosity and the radiation spectrum as seen by a distant observer.

Essentially, by restricting the surface to be sufficiently compact, it is possible to robustly predict the properties of any putative photosphere emission, independent of the specific properties of the radiating surface. Direct flux limits can then be used to constrain and/or exclude the presence of a photosphere.

The above argument has already been successfully employed in the case of Sagittarius A* (Sgr A*), the supermassive black hole at the center of the Milky Way (Narayan et al. 1998; Broderick & Narayan 2006, 2007; Narayan & McClintock 2008; Broderick et al. 2009), where limits on $\dot{M}$ were obtained from the observed bolometric luminosity, assumed to arise from the accretion flow during infall. It was shown that, for physically reasonable radiative efficiencies, it is impossible to accommodate a photosphere. Therefore, Sgr A* must have an event horizon behind which the kinetic energy of the infalling accreting gas is hidden.

The supermassive black hole at the center of the nearby giant elliptical galaxy M87 (which we will refer to as M87* hereafter) is a second target for which the EHT has provided horizon-scale limits upon the extent of its mm-wavelength emission. Here we explore the implications of these and related observations for the existence of an event horizon in M87*. In what follows we assume a mass of $6.16 \times 10^9\, M_\odot$ and distance of 16.5 Mpc for M87*, reported in the recent review by Kormendy & Ho (2013). The mass estimate is based on the stellar dynamical modeling described in Gebhardt et al. (2011), and is roughly a factor of 2 larger than the value obtained by gas dynamical measurements (Walsh et al. 2013); both methods are potentially complicated by the fact that M87* is offset from the center-of-light by as much as 10 pc, impacting the underlying assumptions regarding orbital isotropy (Batcheldor et al. 2010). However, our qualitative conclusions are insensitive to this difference, being marginally stronger with the smaller black hole mass.[12]

M87* is nearly three orders of magnitude more massive than Sgr A*, probing a mass regime more relevant for the bright AGN observed at high redshift. Unlike Sgr A*, whose mm and radio emission seem to be primarily from the accretion flow (Yuan & Narayan 2014), the mm/radio emission of M87* is dominated by a powerful relativistic jet.

Two lines of argument strongly imply that the relativistic jet in M87 originates near the black hole. First, astrometric measurements of the radio core position reveal a wavelength-dependent shift, asymptoting to a fixed position at short wavelengths, consistent with a black hole-launched jet (Hada et al. 2011). Second, the small scales implied by EHT observations at 1.3 mm are commensurate with the scales expected near the black hole (Doeleman et al. 2012, and references therein). This is additionally supported by the success of semi-analytical jet models in simultaneously reproducing the EHT observations, large-scale jet properties, and spectral energy density (SED) of M87, that will be reported elsewhere. Thus, the sub-mm jet is almost certainly launched in the immediate environment of the black hole.

[12] The temperature of a putative surface observed at infinity, defined in Equation (11), depends on the mass as $M^{-1/2}$, and thus is higher for smaller masses. This shifts the resulting emission to higher frequencies where better limits on the observed nuclear emission exist.

All current potential mechanisms for launching relativistic jets invoke an accretion flow. This is trivially true for disk-launched outflows (e.g., Blandford & Payne 1982), but it is also the case for black hole spin-powered jets (e.g., Blandford & Znajek 1977). In the latter case, the accretion disk is needed to confine the horizon-penetrating magnetic flux which enables the black hole's rotational energy to be tapped. While jet efficiencies, defined as $\eta_{\rm jet} \equiv L_{\rm jet}/\dot{M}c^2$ where $L_{\rm jet}$ is the total jet luminosity (radiative, magnetic and mechanical), can instantaneously exceed unity as a result of the electromagnetic tapping of the black hole spin (Tchekhovskoy et al. 2011), instabilities at the jet-disk interface limit how high $\eta_{\rm jet}$ can be in practice. Thus, even for black hole spin-powered jets, $L_{\rm jet}$ may be used to estimate $\dot{M}$, and thus address the existence of an event horizon in M87*.

In Section 2 we describe how the jet power and $\dot{M}$ are related, and obtain an estimate for the latter in M87*. The size constraints placed by mm-VLBI are summarized in Section 3 and the relevant observational flux limits are presented in Section 4. The associated constraints upon the existence of a photosphere are discussed in Section 5. Our conclusions are summarized in Section 6.

2. ESTIMATES OF $\dot{M}$

2.1. Relating $\dot{M}$ to Jet Power

All current models for launching relativistic jets require an accretion disk. In the simplest models, the jet is merely the innermost relativistic part of a magnetocentrifugal wind flowing out from the surface of the disk. In such models (e.g., Blandford & Payne 1982), the jet and the lower-velocity wind are ultimately powered by the gravitational potential energy released by the accreting gas. Thus the jet luminosity is limited by the overall energy efficiency of the disk,

$$\eta_{\rm jet} \equiv \frac{L_{\rm jet}}{\dot{M}c^2} < \frac{L_{\rm jet} + L_{\rm wind} + L_{\rm radiation}}{\dot{M}c^2} = \eta_{\rm disk}, \tag{1}$$

where the disk efficiency $\eta_{\rm disk}$ is determined by the radius of the inner edge of the disk, i.e., the radius $r_{\rm ISCO}$ of the innermost stable circular orbit (ISCO) of the spacetime (Novikov et al. 1973),

$$\eta_{\rm disk} = 1 - \sqrt{1 - \frac{2}{3r_{\rm ISCO}}}. \tag{2}$$

The efficiency $\eta_{\rm disk}$ varies from 0.057 for a non-spinning black hole up to 0.42 for a maximally spinning black hole. A typical value is probably $\sim$0.1−0.2. This means that, for disk-powered jets, the mass accretion rate implied by a given jet luminosity is roughly

$$\dot{M} \approx 10\,\frac{L_{\rm jet}}{c^2}. \tag{3}$$

Alternatively, the jet may be powered by black hole rotation (Blandford & Znajek 1977). In this case, the jet is launched by large-scale ordered magnetic fields that penetrate the horizon, and the total jet power is

$$L_{\rm jet} = \frac{k}{4\pi c}\Omega_H^2\Phi^2, \tag{4}$$

where $\Omega_H \equiv a_* c/2r_+$ is the angular velocity of the horizon, located at $r_+ = (GM/c^2)\,(1 + \sqrt{1 - a_*^2})$ where $a_* = a/M$ is

the dimensionless spin of the black hole, Φ is the magnetic flux threading the horizon, and $k \approx 0.045$ is a dimensionless coefficient that varies modestly with black hole spin (see Tchekhovskoy et al. 2010 for a numerical calculation of this dependence). As Equation (4) shows, the jet power increases quadratically with both black hole spin and magnetic flux. The former is limited by the condition $a_* < 1$, and the latter is limited by the requirement that the magnetic field through the horizon has to be confined by the accretion flow. As a rough estimate, one could say that the accreting gas is virialized and exerts a ram pressure of order

$$P_{\rm acc} \approx \rho v_k^2, \tag{5}$$

where v_k is the local Keplerian velocity. At the disk-funnel interface, assumed to occur at a cylindrical radius $r_{\rm eq}$, the ram pressure must balance the magnetic pressure within the jet, and thus

$$L_{\rm jet} \approx \frac{k\Omega_H^2}{4\pi c}\left(2\pi r_{\rm eq}^2 B_{\rm eq}\right)^2 \approx \frac{2\,kc\pi^2}{r_+^2} r_{\rm eq}^4 \rho_{\rm eq} v_{k,\rm eq}^2, \tag{6}$$

where $B_{\rm eq}$, $\rho_{\rm eq}$, and $v_{k,\rm eq}$ are the magnetic field strength, gas density and Keplerian velocity at $r_{\rm eq}$ and we have assumed $a_* \approx 1$.

At the disk-funnel interface, the heavier gas is supported on top of an otherwise buoyant magnetic field, and thus a balanced configuration is generally unstable. The interchange instability, a close relative to the more commonly discussed Raleigh–Taylor instability, results in the growth of gas fingers that interpenetrate the magnetosphere, allowing accretion to occur on timescales comparable to the Keplerian period at the interface (Spruit et al. 1995; Igumenshchev et al. 2003; Li & Narayan 2004). Therefore, even in the presence of a strong funnel field, the typical accretion rate is

$$\dot{M} \approx 4\pi r_{\rm eq}^2 \rho_{\rm eq} v_{k,\rm eq}, \tag{7}$$

differing from the previous estimate by only a factor of order unity. As a result,

$$\dot{M} \approx 10\,\frac{L_{\rm jet}}{c^2}, \tag{8}$$

i.e., this approximate calculation gives an estimate for $\dot{M}$ not very different from the case of a disk-powered jet (Equation (3)).

Ghosh & Abramowicz (1997) and Livio et al. (1999) studied in greater detail the balance between an accretion disk and a magnetic flux bundle confined around a central black hole and concluded that, for the case of a standard radiatively efficient thin accretion disk, the likely jet efficiency is significantly smaller than 10%, which means that $\dot{M}$ is likely to be substantially larger than $10L_{\rm jet}/c^2$. The situation is, however, different in the case of systems like M87 which have hot advection-dominated accretion flows (for a review, see Yuan & Narayan 2014).

Recent GRMHD simulations (e.g., Tchekhovskoy et al. 2011; McKinney et al. 2012; Narayan et al. 2012; Sądowski et al. 2013) have shown that substantial magnetic flux can be confined around a black hole by a hot accretion flow. The field strength is larger than simple estimates suggest partly because of geometrical factors related to the shape and dynamics of the accretion flow and partly because of relativistic corrections in the vicinity of the black hole horizon (Tchekhovskoy et al. 2015). The net result is that the jet efficiency can be up to a factor of 10 larger than naive estimates suggest. Indeed efficiencies exceeding 100% are possible if the black hole spins at close to the maximal rate and the magnetic flux achieves its maximum value via a magnetically arrested disk (MAD, Narayan et al. 2003; Tchekhovskoy et al. 2011) configuration. Allowing for these effects, we thus have

$$\dot{M} \gtrsim \frac{1}{2}\frac{L_{\rm jet}}{c^2}, \tag{9}$$

where the value we give for the coefficient is highly conservative. In the following, we make the conservative assumption that $\dot{M} = L_{\rm jet}/2c^2$.

2.2. Estimates of Jet Power in M87

A variety of estimates of M87's jet power may be found in the literature, covering a wide variety of distances from the black hole and thus timescales probed. All the estimates are consistent with a jet power of roughly 10^{44} erg s^{-1}.

Surrounding M87 is an extended radio-bright structure (Bolton et al. 1949; Mills 1952; Baade & Minkowski 1954), reaching radial distances of nearly 30 kpc, and believed to be powered by the central AGN (Owen et al. 2000). Estimates of the jet power may be obtained by estimating the energy required to grow the radio halo and dividing it by the buoyancy timescale; this gives $L_{\rm jet} \approx$ few $\times\, 10^{44}$ erg s^{-1} (Owen et al. 2000). Recent efforts to estimate the synchrotron age of the halo using LOFAR observations give roughly 40 Myr, resulting again in $L_{\rm jet} \approx 6$–10×10^{44} erg s^{-1}, depending on the assumed particle content (de Gasperin et al. 2012). These necessarily represent estimates averaged over the buoyancy time at 10 kpc, roughly 10 Myr. As a result, inferring the current instantaneous jet power requires some assumption regarding the recent history of activity in M87.

Like many radio-loud AGN, on kpc scales M87 exhibits X-ray cavities and regions of enhanced emission associated with shocks. These are presumed to be driven by the AGN jet, and thus provide an additional measure of jet power. Estimates of the shock energetics alone require a power source of 2.4×10^{43} erg s^{-1} (Forman et al. 2005, 2007). The power inferred from the nearby cavity inflation is sensitively dependent on the gas pressure profile, and estimates range from 10^{43} to 10^{44} erg s^{-1} (Young et al. 2002; Allen et al. 2006; Rafferty et al. 2006). Again, these are time-averaged over the buoyancy time, in this case roughly ~1 Myr because of the smaller scale (1 kpc), with the attendant caveats regarding variability.

Knot A is a bright optical feature within the jet at a projected distance of approximately 0.9 kpc. While comparable to the distance of the closest cavities, knot A is one of a number of superluminal features within the jet, with apparent velocities of up to $1.6c$, implying that it moves relativistically (Meyer et al. 2013). Interpreting knot A as an oblique shock within the jet results in a jet power estimate of $(1$–$3) \times 10^{44}$ erg s^{-1} (Bicknell & Begelman 1996); values much in excess of this are expected to over-produce the emission at knot A (Reynolds et al. 1996). Equally

importantly, the time delays associated with estimates from knot A are roughly 2×10^3 years, three orders of magnitude shorter than those associated with the large-scale radio and X-ray morphology.

Finally, located at a projected distance of 60 pc from M87* is the *HST*-1 complex, comprised of stationary and superluminal components with apparent velocities of up to $6c$ (Biretta et al. 1999; Giroletti et al. 2012). At these distances, *HST*-1 provides the most contemporaneous estimates of the jet power, with a time delay of roughly 30 years. If identified with a recollimation shock, the stationary component of *HST*-1 implies a jet power of $\approx 10^{44}$ erg s^{-1} (Stawarz et al. 2006). This is grossly consistent with estimates obtained when the shock structure is modeled in more detail (Bromberg & Levinson 2009).

Overall, the typical estimate for the bolometric power of M87's jet is $\sim 10^{44}$ erg s^{-1}, with perhaps a factor of few uncertainty. The implied mass accretion rate is $\dot{M} \sim 10^{-3}\, M_\odot$ yr^{-1}. This is roughly consistent with the upper limit on the near-horizon accretion rate obtained via Faraday rotation which find $9.2 \times 10^{-4}\, M_\odot$ yr^{-1} within a radius of $\approx 40GM/c^2$, assuming that the Faraday screen lies within a radiatively inefficient accretion flow (Kuo et al. 2014).

3. 1.3 MM VLBI SIZE OF M87

The detection of emission at the core of M87 on the scale of several times the Schwarzschild radius is robust. Observations on an array including telescopes in California (CARMA), Hawaii (JCMT) and Arizona (SMT) provided projected baseline lengths ranging from $6 \times 10^8\lambda$ to $3.4 \times 10^9\lambda$. Firm detection of M87 on the longest baselines alone requires the existence of compact structure with an upper size limit of $\sim$60 microarcseconds, corresponding to a diameter of $\sim 16GM/c^2$ at the presumed mass and distance of M87. When modeled as a single circular Gaussian brightness distribution (Doeleman et al. 2012), the FWHM is $11 \pm 1GM/c^2$ with calibration errors included in the 3σ parameter estimate.

Other instrumental factors can affect the estimated 1.3 mm VLBI size but were determined to be negligible. These include the stability of hydrogen maser frequency standards used at each VLBI station and the polarization purity of the telescope receivers which were configured for Left Circular Polarization. On short ($\approx$1 s) timescales, the Masers were compared to ultra-stable quartz oscillators, and longer-term stability was determined through timing comparisons with GPS. Polarization characteristics at each antenna were determined by injecting known polarization signals into the receiver feeds at the single dish sites, and through separate polarization calibration observations at CARMA.

The main source of uncertainty in the true size and shape of the compact 1.3 mm emission is the limited VLBI baseline coverage, which is insufficient to exactly determine the brightness morphology. The VLBI data can also be fitted, for example, with a uniform disk of diameter $16.4GM/c^2$, comparable to that inferred from the the long-baseline correlated flux measurements alone. In this work we adopt the circular Gaussian diameter of $11GM/c^2$ with the proviso that future EHT observations with improved Global coverage will be able to image and model M87 in detail. The disk and more complex models typically predict "nulls" in the VLBI signal as a function of baseline length that are not yet seen, but which may emerge as EHT sites enabling longer baselines are added to the array.

Doeleman et al. (2012) associate the 1.3 mm compact emission with the ISCO of the M87 black hole, enlarged by the strong gravitational lensing that occurs at small radii. Location of this emission close to, or at, the black hole is supported by phase referenced multi-frequency VLBI observations at longer wavelengths, which show the core of M87 to shift toward a convergent point with shorter observing wavelength (Hada et al. 2011). Extrapolation of this shift to the observed size at 1.3 mm places the emission within a few Schwarzschild radii of the black hole, making the derived 1.3 mm size a good estimate for the photosphere of a putative surface.

While it is possible that the 1.3 mm emission arises some distance from the black hole, the EHT-derived size can still serve as an upper limit on the spatial extent of an intrinsic photosphere. Theoretical models of electromagnetic jets, both semi-analytical estimates and numerical simulations, uniformly show an expanding jet width profile with increased distance from the central engine. These expectations are quantitatively consistent with jet observations on scales covering six orders of magnitude (Hada et al. 2013; Nakamura & Asada 2013) confirm a parabolic jet shape to within $\sim 20GM/c^2$ of the black hole. There is, in short, no compelling mechanism to suggest that an electromagnetic jet launched from a photosphere later converges to a markedly smaller size.

4. THE SED OF THE NUCLEAR AGN SOURCE IN M87

Tables 1 and 2 list the optical and near-infrared SED data that are used in Figures 1 and 2. Table 2 lists the measurements made in the Perlman et al. (2011) five year campaign to measure nuclear variability. Table 1 lists the rest of the data.

Most flux measurements were made with the *Hubble Space Telescope* (*HST*) and various imaging cameras. Also, unless otherwise noted, nuclear flux measurements were made using a correction for the galaxy light under the central point-spread function (PSF) that is based on measuring and fitting the profile at larger radii (see, e.g., Lauer et al. 1992; Sparks et al. 1996). Various profile fit models such as Sérsic functions (Sérsic 1968) and ones with a core (see Lauer et al. 1995) are used. Also unless otherwise noted, the innermost jet knot *HST*-1 is not included in the measurements, although faint extensions of the jet at smaller radii are included (see, e.g., Sparks et al. 1996; Perlman et al. 2001). The measurements are discussed in their source papers. A few details are noteworthy here:

An estimate by Young et al. (1978) of $V \simeq 16.69 \pm 0.05$ (see Lauer et al. 1992) corresponding to $F_\nu = 0.80 \pm 0.04$ mJy is consistent with the results in Table 1 but is not used in this paper. The epoch was 1975 March 14–1977 May 22 and the Palomar Observatory 200-inch Hale telescope was used. We omit this measurement because the seeing FWHM was $1''$ to $2''$—hence the exclusion of jet knots is uncertain—and because the galaxy subtraction was not consistent with our *HST*-era understanding of the cuspy cores of elliptical galaxies (e.g., Lauer et al. 1992, 1995).

The Lauer et al. (1992) *HST* PC F785LP images ($\lambda_{\rm eff} = 8900$ Å) were taken with the unrefurbished *HST* but

Table 1
Ultravoilet–Infrared SED of the M87 Nuclear Source

λ (μm) (1)	log ν (Hz) (2)	F_ν (mJy) (3)	σ_F (mJy) (4)	Epoch (5)	Program *HST* ID (6)	Camera (7)	Source (8)
0.1255	15.38	0.162	0.032	1991 Apr 6	1228	FOC	Sparks et al. (1996)
0.1507	15.30	0.081	0.016	1991 Apr 5	1228	FOC	Sparks et al. (1996)
0.1585	15.28	0.068	0.014	1991 Jun 23	1517	FOC	Sparks et al. (1996)
0.23	15.11	0.158	0.032	1991 Apr 5	1228	FOC	Sparks et al. (1996)
0.25	…	0.1153	0.0014	2003 Mar 31	9454	ACS HRC	Maoz et al. (2005)
0.25	…	0.1119	0.0014	2003 Dec 10	9454	ACS HRC	Maoz et al. (2005)
0.2475	…	0.089	0.009	1999 May 17	8140	STIS NUV-MAMA	Chiaberge et al. (2002)
0.299	…	0.198	0.005	1998 Feb 25	6775	WFPC2 PC	This paper; Perlman et al. (2001)
0.33	…	0.1759	0.0019	2003 Mar 31	9454	ACS HRC	Maoz et al. (2005)
0.33	…	0.1743	0.0019	2003 Dec 10	9454	ACS HRC	Maoz et al. (2005)
0.3708	14.91	0.457	0.091	1991 Jun 23	1517	FOC	Sparks et al. (1996)
0.456	…	0.493	0.012	1998 Feb 25	6775	WFPC2 PC	This paper; Perlman et al. (2001)
0.5017	14.78	1.02	0.20	1991 Apr 5	1228	FOC	Sparks et al. (1996)
0.541	…	0.637	0.059	1991 Feb 24	1105	WF/PC PC	Lauer et al. (1992); this paper
0.600	…	0.787	0.020	1998 Feb 25	6775	WFPC2 PC	This paper; Perlman et al. (2001)
0.801	…	1.063	0.027	1998 Feb 25	6775	WFPC2 PC	This paper; Perlman et al. (2001)
0.801	…	0.759	0.076	1999 May 11	8140	WFPC2	Chiaberge et al. (1999, 2002)
0.8900	…	0.81	…	1991 Jun 1	3242	WF/PC PC	Lauer et al. (1992)
1.2	…	2.45	0.69	1993 Jun 1	…	ESO/MPI 2 m	Stiavelli et al. (1997)
1.60	…	3.02	0.15	1997 Nov 20	7171	NICMOS NIC2	Baldi et al. (2010)
2.201	…	2.28	0.60	1994 Apr 3	…	UKIRT 3.8 m	Stiavelli et al. (1997)

Note. Columns (1) and (2) are the effective, pivot, or median wavelength and frequency of the photometric bandpass. Columns (3) and (4) are the measured flux and its 1σ error. Because the nuclear source flux is time-variable, Column (5) gives the epoch of the observation. This is not used in the present paper: all SED points are plotted in Figure 1 to provide an illustration of the amplitude of variation. This amplitude is in general larger than the errors of the SED measurements. Column (6) provides the *HST* proposal ID, and Column (7) lists the *HST* camera or the telescope used. Column (8) gives the source of the measurement.

Table 2
Ultravoilet–Optical SED of the M87 Nuclear Source from Perlman et al. (2011)

F_ν (mJy) F606W 0.589 μm (1)	F_ν (mJy) F330W 0.336 μm (2)	F_ν (mJy) F250W 0.272 μm (3)	F_ν (mJy) F220W 0.226 μm (4)	Epoch (5)	Program *HST* ID (6)	Camera (7)
0.671 ± 0.007	0.305 ± 0.002	…	0.146 ± 0.011	2002 Dec 7	9705	ACS HRC
0.630 ± 0.006	0.305 ± 0.002	…	0.146 ± 0.011	2002 Dec 10	9493	ACS HRC
0.478 ± 0.005	…	…	0.137 ± 0.011	2003 Nov 29	9829	ACS HRC
1.066 ± 0.011	0.475 ± 0.002	0.306 ± 0.014	0.226 ± 0.014	2004 Nov 28	10133	ACS HRC
1.306 ± 0.013	…	0.363 ± 0.010	…	2004 Dec 26	10133	ACS HRC
0.891 ± 0.009	…	0.280 ± 0.009	…	2005 Feb 9	10133	ACS HRC
1.037 ± 0.010	…	0.328 ± 0.010	…	2005 Mar 27	10133	ACS HRC
0.932 ± 0.009	0.446 ± 0.003	0.274 ± 0.009	0.217 ± 0.009	2005 May 9	10133	ACS HRC
0.839 ± 0.008	…	0.273 ± 0.009	…	2005 Jun 22	10133	ACS HRC
0.639 ± 0.006	…	0.192 ± 0.007	…	2005 Aug 1	10133	ACS HRC
0.735 ± 0.007	0.349 ± 0.002	0.217 ± 0.008	0.170 ± 0.008	2005 Nov 29	10133	ACS HRC
0.756 ± 0.008	…	0.234 ± 0.008	…	2005 Dec 26	10617	ACS HRC
0.631 ± 0.006	…	0.201 ± 0.008	0.160 ± 0.008	2006 Feb 8	10617	ACS HRC
0.780 ± 0.008	…	0.232 ± 0.008	…	2006 Mar 30	10617	ACS HRC
0.862 ± 0.009	0.372 ± 0.002	0.193 ± 0.007	0.1564 ± 0.007	2006 May 23	10617	ACS HRC
1.370 ± 0.014	0.636 ± 0.003	0.323 ± 0.009	…	2006 Nov 28	10910	ACS HRC
1.006 ± 0.010	…	0.276 ± 0.009	…	2006 Dec 30	10910	ACS HRC
1.292 ± 0.017	…	…	…	2007 Nov 25	11216	WFPC2 WFC

Note. The first four columns list fluxes F_ν (mJy) for the four filters and their pivot wavelengths as listed in the table headers. Columns (5)–(7) are explained in their headers.

allow a clear separation of the nuclear AGN from the innermost jet knots N1 and M at $\sim 0\farcs1$ and $\sim 0\farcs18$ from the center (see their Figure 5). These knots are included in most *HST* photometry and all ground-based photometry. Lauer et al. (1992) measure them separately and show that, at 8900 Å and on 1999 June 1, the nucleus contributed 89% of the combined

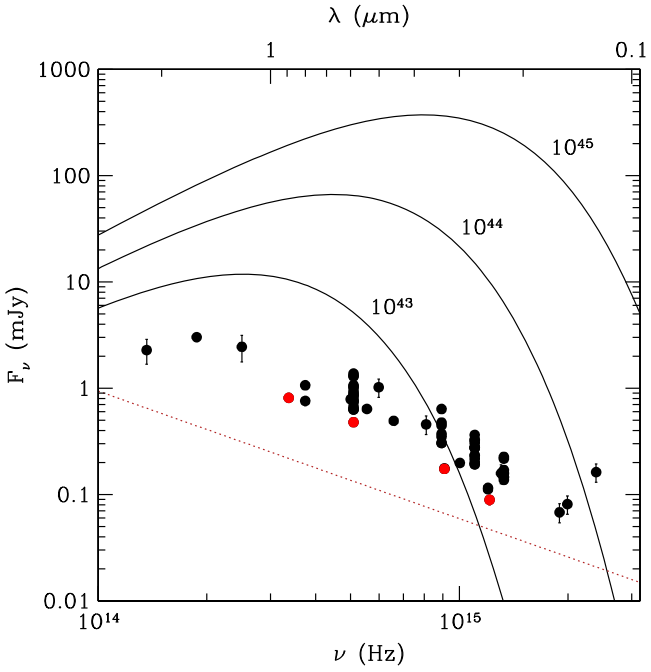

Figure 1. Inferred infrared-optical spectrum from a putative photosphere for $L_{\rm photo} = 10^{43}, 10^{44}$, and 10^{45} erg s^{-1} (solid lines, from bottom to top) compared to the empirical limits on the SED of M87* listed in Tables 1 and 2 (colored dots). The dark-red dotted line indicates the estimated limit arising from the intrinsic jet spectrum, and thus presumably the confusion limit. All points in Table 2 are plotted in order to provide some indication of the variability of the source. Those data that provide the constraints presented in Figure 2 are shown in red. Note that photospheric emission at a level of 10^{44} erg s^{-1}, as expected based on current estimates of the jet power (§2), is ruled out with high confidence.

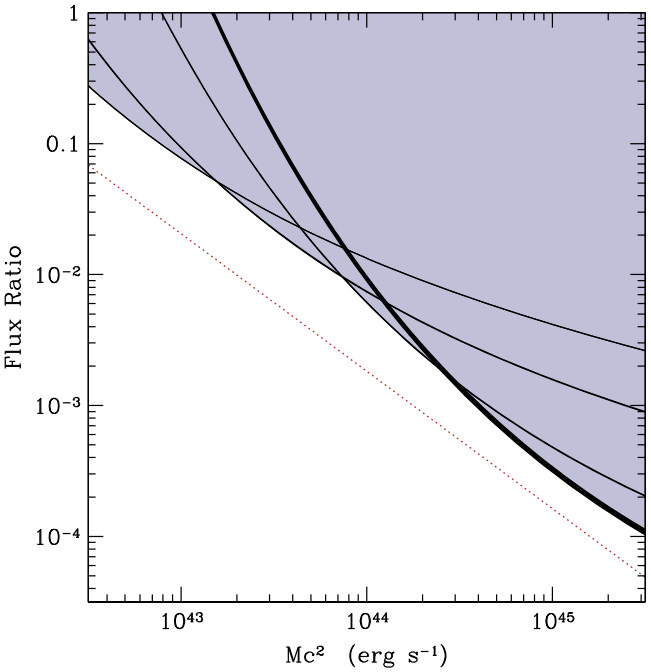

Figure 2. Ratio of the measured fluxes to that inferred from a putative photosphere. The thick black lines indicate the constraint implied by the individual flux measurements shown in red in Figure 1, corresponding to those that dominate the constraint at some $\dot{M}$ in the range presented. The line widths indicate the 1σ upper limit and the grayed region is the area excluded by the aggregate. The dark-red dotted line indicates the estimated limit arising from the intrinsic jet spectrum, and thus presumably the confusion limit.

flux including N1 and M. We have used their measurement of the nuclear flux at 8900 Å. They also measure the total flux of the nucleus plus N1 plus M in the F555W band at almost the same time as the F785LP measurements. We assume that the fraction of this total that comes from the nucleus is also 89% and correct their total measurement to a nuclear estimate of 0.637 mJy. This correction has not been applied to any other measurements, because we cannot know the variability of the nucleus, of N1, and of M separately. All these other measurements include the innermost part of the jet interior to knot *HST*-1.

We repeated the F55W galaxy subtraction to get the estimated error ±0.059 on the F555W flux.

The Sparks et al. (1996) measurements were made with pre-COSTAR *HST* using the ground-based photometry by Young et al. (1978) as the galaxy model. The latter is probably not a problem; they note that corrections for galaxy light are small. If the former is a problem, then light at large radii in the PSF could be missed and the measurements could be lower limits on fluxes. However, we emphasize that this problem is almost certainly much smaller than the intrinsic variability amplitude of the nuclear source.

Sparks et al. (1996) measured the nuclear AGN in *J* and *K* bands using the ESO/MPI 2 m telescope and the United Kingdom Infrared Telescope (UKIRT: 3.8 m), respectively. Galaxy light underlying the AGN was removed using an iterative procedure to separate the stellar brightness profile from the central source. That source was measured inside a 2.″8-diameter aperture, i.e., one that is large enough to include jet knot *HST*-1. The knot is not visible in their image, and the higher-resolution *HST* images in Sparks et al. (1996) suggest that it contributed negligibly at that time. There are jet components closer to the center (e.g., Lauer et al. 1992); these are included even in most *HST* measurements. We therefore use the Sparks et al. (1996) measurements as published.

The Chiaberge et al. (1999, 2002) measurements were made by subtracting from the nuclear flux the galaxy flux at radius 0.″23 in the *R* band and at radius 0.″17 in the ultraviolet band. Since the galaxy's profile is a shallow power law inside the cuspy core (Lauer et al. 1992), the resulting fluxes are strictly speaking upper limits. However, the galaxy contribution to the measurements is smaller than the amplitude of the variability of the M 87 nuclear source.

The four *HST* WFPC2 points from this paper were measured by E.S.P. following the procedures of Perlman et al. (2001) in February of 1998. Knot *HST*-1 was about 1% of the central source at this time and is not included in the measurement. Prior to measuring the nuclear flux, a galaxy model (made with the IRAF tasks `ellipse` and `bmodel`) was subtracted from each of these images. The Perlman et al. (2011) measurements listed in Table 2 were made in the same way.

We have not included the UV photometry of the nucleus published by Madrid (2009) because all of those fluxes have been referenced to a single wavelength based on an unpublished spectral model. Instead, we use the measurements published by Perlman et al. (2011), which include all of the epochs between 2004 and 2006 that were included in Madrid (2009) but does not apply any spectral model in their calibration. It should be noted that when the spectral referencing applied by Madrid (2009) is removed, the measurements of Perlman et al. (2011) and Madrid (2009)

agree to within the errors (J. Madrid 2011, private communication).

5. PHOTOSPHERE EMISSION

Were a photosphere present in M87* instead of a horizon, it would be heated by the constant deposition of kinetic energy from the accretion, resulting in an additional component in the spectrum. Since the infall time is only logarithmically dependent upon the photosphere redshift, it is natural to assume that the surface will reach a steady state in which the emitted luminosity and the impinging kinetic power from the accretion flow are balanced.

The gravitational binding energy liberated per unit time by the infalling material necessarily depends on the size of the putative photosphere, approaching $\dot{M}c^2$ for radii comparable to that of the horizon. That is, typically,

$$L_{\rm surf} \approx \frac{GM}{c^2 R}\dot{M}c^2, \tag{10}$$

where R is the radius of the surface.[13]

The radius of any such surface is strongly limited by the 1.3 mm VLBI observations discussed in Section 3. These already constrain the 1.3 mm emission region to within the vicinity of the photon orbit, expected to have a diameter of roughly $10.4GM/c^2$ in projection and depending very weakly on the assumed black hole spin.[14] Moreover, at millimeter wavelengths and longer M87 still exhibits the flat radio spectrum indicative of a self-absorbed synchrotron jet (see, e.g., Blandford & Königl 1979). This interpretation receives strong support from the evolution of the radio core location with wavelength, with the offset evolving $\propto\lambda^{0.94\pm0.09}$, presumably due to the shrinking of the photosphere (Hada et al. 2011). Thus, at infrared and optical wavelengths the size of the photosphere is expected to be smaller than the $\sim 11GM/c^2$ limit from the mm-VLBI observations described in Section 3—if the optically thick to thin transition completes at a wavelength of 1.1 mm or shorter, this will lie within the projected photon orbit. This conclusion is only strengthened if the emission arises from a significant distance from the central engine, as described in Section 3.

However, the efficiency with which the jet is driven depends on the surface in a similar fashion, becoming larger for more compact objects. For disk driven jets, the surface and jet efficiences are approximately equal (see Equation (1)), implying that $L_{\rm surf} \approx L_{\rm jet}$. For black hole rotation driven jets the efficiency scales roughly as v_k due to the competition between the lower Ω_H and higher Φ as the surface increases in size (see the Appendix). As a result, once again $L_{\rm surf} \approx L_{\rm jet}$, with an additional factor of order unity that depends only very weakly on the photosphere size. Thus, here we make the conservative assumption that $L_{\rm surf} \approx L_{\rm jet}/2$ as described in Equation (9).

[13] While quantitative variations from the Newtonian expressions do occur for high-redshift objects, these are qualitatively similar, differing by a factor of order unity that depends primarily on the dynamical state of the infalling gas (see, e.g., Broderick et al. 2009, and Equation (3)).

[14] While it is true that the projected photon orbit viewed from the equatorial plane can shrink to $9GM/c^2$ for maximally spinning black holes, this is not the case at small inclinations; at the estimated inclination of $<25°$ of the M87*'s jet (Heinz & Begelman 1997), and thus presumably spin inclination, spin has negligible impact on the projected photon orbit size.

Since the size constraints placed by EHT observations at 1.3 mm already limit the size of any putative photospheric emission in M87* to scales comparable to, or smaller than, the photon orbit, the photosphere will necessarily be thermalized by the strong lensing, resulting in a gravitational analog of the standard blackbody cavity (see the discussion in Broderick & Narayan 2006, 2007). Thus, surface should be temperature as seen by a distant observer is related to the accretion rate via

$$4\pi R_a^2 \sigma T_\infty^4 \approx \frac{L_{\rm jet}}{2} \quad \rightarrow \quad T_\infty \approx \left(\frac{L_{\rm jet}}{8\pi R_a^2 \sigma}\right)^{1/4}, \tag{11}$$

where σ is the Stefan–Boltzmann constant and $R_a \approx 5GM/c^2$ is the apparent radius of any object lying within the photon orbit. Note that the temperature estimate depends only weakly on $\dot{M}$, and thus on the uncertainties associated with the jet power and jet efficiency. For the accretion rate inferred in Section 2 for M87*, $T_\infty \approx 8.5 \times 10^3$ K, which means that the surface emission will peak in the optical band. The observed spectral flux from the surface is given by

$$F_{\nu,\rm ph} = \frac{R_a^2}{D^2}\frac{2h\nu^3/c^2}{e^{h\nu/kT_\infty} - 1}, \tag{12}$$

where D is the distance to M87. This predicted flux may be directly compared to observations and thereby we can hope to constrain whether or not M87* has a surface.

6. DISCUSSION

A direct comparison of the putative photosphere spectrum to the measured fluxes listed in Table 1 is shown in Figure 1. Because of the intrinsic uncertainty in $\dot{M}$, we show predicted spectra spanning a wide range of $\dot{M}$, corresponding to variations in the jet efficiency or measured jet power. In all cases, photospheric emission is excluded at high confidence. This conclusion is further supported by Figure 2 which shows the ratio of the measured fluxes to that implied by a photosphere as a function of $\dot{M}$. At all physically reasonable accretion rates the measured fluxes lie at least an order of magnitude below that required in the absence of an event horizon.

Improvements in the measured flux limits will necessarily result in increased confidence with which any photospheric emission may be ruled out. However, the intrinsic emission from the observed jet component provides a natural limit. Assuming a spectral index of 1.2, consistent with a transition from optically thick to optically thin near 1mm and the optical flux limits, we estimate the corresponding floors on the infrared-optical spectrum and flux ratio, shown by the dotted, dark-red lines in Figures 1 and 2, below which the emission from the jet-launching region must be modeled in detail. Note that this is rather uncertain; variations in the spectral index between the core and larger scale jet emission arising, e.g., from an evolution in the relativistic particle distributions, could easily harden the core spectrum sufficiently to fully account for the vast majority of the fluxes shown in Figure 1. Nevertheless, even if this is not the case, it appears that the current flux limits are within an order of magnitude of the confusion limit, below which careful modeling of the jet emission will be required to obtain stronger constraints.

Despite the astrophysical uncertainty in the relationship between the jet power and mass accretion rate, we have shown

in this paper that, within the context of current jet launching paradigms, we can rule out the existence of an observable photosphere in M87* within which the kinetic energy of the accreting gas is deposited. The implication is that the kinetic energy of the gas is advected past an event horizon, beyond which it is no longer visible to distant observers. In other words, M87* must have an event horizon.

This argument may be evaded in a variety of ways, though all require speculative new physics and most invoke black hole alternatives. First, M87* could fail to reach steady state, preventing the use of the accretion rate as a proxy for the surface luminosity. This requires unphysically high heat capacities (which the gravastar model of Mazur & Mottola 2004 apparently does possess, see Chapline et al. 2005), already excluded in many cases (Broderick & Narayan 2007), or exotic alternatives like suitably tuned wormholes (e.g., Damour & Solodukhin 2007). Second, the surface could fail to thermalize, though this is strongly argued against by the compact emission observed at millimeter wavelengths, and may be excluded altogether by the development of a baryonic atmosphere. Third, the efficiency factor could be much larger than implied by current jet launching models, requiring mechanisms qualitatively different from those currently favored. For example, if M87* were a rapidly spinning compact object with a strong magnetic field, the accreting gas could be stopped at a magnetospheric radius and flung out in a jet without any gas reaching the underlying photosphere (e.g., the neutron star propeller model of Illarionov & Sunyaev 1975). In any such model, the magnetospheric radius can be only slightly larger than the surface of the central object (because of the VLBI constraints on the angular size of the source), and it seems likely that a lot of accreting gas will penetrate through the magnetosphere and reach the surface (e.g., Kulkarni & Romanova 2008). In addition, the material that is stopped and flung out by the magnetosphere is likely to dissipate a good fraction of its kinetic energy where it meets the rotating magnetosphere, resulting in thermalized radiation not very different from that expected from a photosphere. We regard this propeller model as strictly physically possible but astrophysically implausible. Thus, our argument will be strengthened in the near future as key components to the current jet paradigm are critically tested by mm-VLBI observations of M87.

Based on observations made with the Event Horizon Telescope and the NASA/ESA *Hubble Space Telescope*. The Event Horizon Telescope is supported through grants from the US National Science Foundation, by the Gordon and Betty Moore Foundation (GBMF3561), and through generous equipment donations from the Xilinx Corporation and the HGST company. The NASA/ESA *Hubble Space Telescope* observations were obtained at the Space Telescope Science Institute, which is operated by AURA, Inc., under NASA contract NAS 5-26555. These observations are associated with program numbers 1105, 1228, 1517, 3242, 6775, 7171, 8140, 9454, 9493, 9705, 9829, 10133, 10617, 10910, and 11216. A. E.B. receives financial support from Perimeter Institute for Theoretical Physics and the Natural Sciences and Engineering Research Council of Canada through a Discovery Grant. R.N. received partial supported from the NSF via grant AST1312651 and NASA via grant NNX14AB47G. R.N. also thanks the Perimeter Institute for hospitality while some of this work was carried out. The authors are grateful to Sera Markoff and Brian McNamara for helpful conversations. This work would not have been practical without extensive use of the NASA/IPAC Extragalactic Database (NED), which is operated by the Jet Propulsion Laboratory and the California Institute of Technology under contract with NASA. We also made extensive use of NASA's Astrophysics Data System bibliographic services. J.K.'s work was supported in Texas by the Curtis T. Vaughan, Jr. Centennial Chair in Astronomy and in Germany by a Faculty Research Assignment from the University of Texas and by the Max-Planck-Institut für Extraterrestrsiche Physik (MPE), Garching-by-Munich, Germany. J.K. warmly thanks Director Ralf Bender and the staffs of the MPE and the Universitäts-Sternwarte, Ludwig-Maximilians-Universität, Munich for their hospitality and support during the 2014 visit when most of his work on this paper was done.

Facilities: EHT (JCMT, CARMA, SMA, ARO SMT), *HST* (ACS, FOC, NICMOS, STIS, WFPC1, WFPC2), UKIRT (IRCAM3), Max Planck: 2.2 m (IRAC2)

APPENDIX
BLANDFORD–ZNAJEK JET EFFICIENCY FOR SURFACES

The relationships between accretion rate and both surface luminosity and jet power are dependent upon the assumed surface size. In detail this depends upon the specific jet launching mechanism assumed. Here we consider the question in the context of Blandford–Znajek jets, for which the jet luminosity is related to the properties of the central object via Equation (4). For an object with a large surface there are two important modifications: the angular velocity is limited to $\Omega_H < c/R$, and $\Phi < 2\pi R^2 B_{\rm eq}$. Thus,

$$L_{\rm jet} \lesssim \pi k c R^2 B_{\rm eq}^2 \approx 2\pi k \frac{v_{k,\rm eq}}{c} \dot{M} c^2, \tag{13}$$

where we assumed $\dot{M} \approx 4\pi R^2 \rho_{\rm eq} v_{k,\rm eq}$ and equipartion near the surface (i.e., $r_{\rm eq} \approx R$). This must be compared to

$$L_{\rm surf} \approx \frac{GM}{c^2 R} \dot{M} c^2 \approx \dot{M} v_{k,\rm eq}^2, \tag{14}$$

which gives

$$\frac{L_{\rm surf}}{L_{\rm jet}} \approx \frac{1}{2\pi k} \frac{v_{k,\rm eq}}{c} \propto \left(\frac{GM}{c^2 R}\right)^{1/2}. \tag{15}$$

This is a weak function of R. For the range of surface radii consistent with the recent mm-VLBI limits, it introduces at most a factor of two.

REFERENCES

Allen, S. W., Dunn, R. J. H., Fabian, A. C., Taylor, G. B., & Reynolds, C. S. 2006, MNRAS, 372, 21
Almheiri, A., Marolf, D., Polchinski, J., & Sully, J. 2013, JHEP, 2, 62
Baade, W., & Minkowski, R. 1954, ApJ, 119, 215
Baldi, R. D., Chiaberge, M., Capetti, A., et al. 2010, ApJ, 725, 2426
Batcheldor, D., Robinson, A., Axon, D. J., Perlman, E. S., & Merritt, D. 2010, ApJL, 717, L6
Bicknell, G. V., & Begelman, M. C. 1996, ApJ, 467, 597
Biretta, J. A., Sparks, W. B., & Macchetto, F. 1999, ApJ, 520, 621
Blandford, R. D., & Königl, A. 1979, ApJ, 232, 34
Blandford, R. D., & Payne, D. G. 1982, MNRAS, 199, 883
Blandford, R. D., & Znajek, R. L. 1977, MNRAS, 179, 433
Bolton, J. G., Stanley, G. J., & Slee, O. B. 1949, Natur, 164, 101

Broderick, A. E., Loeb, A., & Narayan, R. 2009, ApJ, 701, 1357
Broderick, A. E., & Narayan, R. 2006, ApJL, 638, L21
Broderick, A. E., & Narayan, R. 2007, CQGra, 24, 659
Bromberg, O., & Levinson, A. 2009, ApJ, 699, 1274
Chapline, G. 2005, in 22nd Texas Symp. on Relativistic Astrophysics, ed. P. Chen et al., 101
Chiaberge, M., Capetti, A., & Celotti, A. 1999, A&A, 349, 77
Chiaberge, M., Macchetto, F. D., Sparks, W. B., et al. 2002, ApJ, 571, 247
Damour, T., & Solodukhin, S. N. 2007, PhRvD, 76, 024016
de Gasperin, F., Orrú, E., Murgia, M., et al. 2012, A&A, 547, A56
Doeleman, S. 2010, in 10th European VLBI Network Symp. and EVN Users Meeting: VLBI and the New Generation of Radio Arrays, 53
Doeleman, S., Agol, E., Backer, D., et al. 2009, in astro2010: The Astronomy and Astrophysics Decadal Survey, Vol. 2010, 68
Doeleman, S. S., Weintroub, J., Rogers, A. E. E., et al. 2008, Natur, 455, 78
Doeleman, S. S., Fish, V. L., Schenck, D. E., et al. 2012, Sci, 338, 355
Done, C., & Gierliński, M. 2003, MNRAS, 342, 1041
Fish, V. L., Doeleman, S. S., Beaudoin, C., et al. 2011, ApJL, 727, L36
Forman, W., Jones, C., Churazov, E., et al. 2007, ApJ, 665, 1057
Forman, W., Nulsen, P., Heinz, S., et al. 2005, ApJ, 635, 894
Garcia, M. R., McClintock, J. E., Narayan, R., et al. 2001, ApJL, 553, L47
Gebhardt, K., Adams, J., Richstone, D., et al. 2011, ApJ, 729, 119
Ghosh, P., & Abramowicz, M. A. 1997, MNRAS, 292, 887
Giroletti, M., Hada, K., Giovannini, G., et al. 2012, A&A, 538, L10
Hada, K., Doi, A., Kino, M., et al. 2011, Natur, 477, 185
Hada, K., Kino, M., Doi, A., et al. 2013, ApJ, 775, 70
Heinz, S., & Begelman, M. C. 1997, ApJ, 490, 653
Igumenshchev, I. V., Narayan, R., & Abramowicz, M. A. 2003, ApJ, 592, 1042
Illarionov, A. F., & Sunyaev, R. A. 1975, A&A, 39, 185
Kormendy, J., & Ho, L. C. 2013, ARA&A, 51, 511
Kulkarni, A. K., & Romanova, M. M. 2008, MNRAS, 386, 673
Kuo, C. Y., Asada, K., Rao, R., et al. 2014, ApJL, 783, L33
Lauer, T. R., Ajhar, E. A., Byun, Y.-I., et al. 1995, AJ, 110, 2622
Lauer, T. R., Faber, S. M., Lynds, R. C., et al. 1992, AJ, 103, 703
Li, L.-X., & Narayan, R. 2004, ApJ, 601, 414
Livio, M., Ogilvie, G. I., & Pringle, J. E. 1999, ApJ, 512, 100
Madrid, J. P. 2009, AJ, 137, 3864
Maoz, D., Nagar, N. M., Falcke, H., & Wilson, A. S. 2005, ApJ, 625, 699
Mathur, S. D. 2011, CQGra, 28, 125010
Mathur, S. D. 2014, IJMPD, 23, 1442024
Mazur, P. O., & Mottola, E. 2004, PNAS, 101, 9545
McKinney, J. C., Tchekhovskoy, A., & Blandford, R. D. 2012, MNRAS, 423, 3083
Meyer, E. T., Sparks, W. B., Biretta, J. A., et al. 2013, ApJL, 774, L21
Mills, B. Y. 1952, Natur, 170, 1063
Nakamura, M., & Asada, K. 2013, ApJ, 775, 118
Narayan, R., Garcia, M. R., & McClintock, J. E. 1997, ApJL, 478, L79
Narayan, R., & Heyl, J. S. 2002, ApJL, 574, L139
Narayan, R., Igumenshchev, I. V., & Abramowicz, M. A. 2003, PASJ, 55, L69
Narayan, R., Mahadevan, R., Grindlay, J. E., Popham, R. G., & Gammie, C. 1998, ApJ, 492, 554
Narayan, R., & McClintock, J. E. 2008, NewAR, 51, 733
Narayan, R., Sądowski, A., Penna, R. F., & Kulkarni, A. K. 2012, MNRAS, 426, 3241
Novikov, I. D., & Thorne, K. S. 1973, in Black Holes (Les Astres Occlus), ed. C. Dewitt, & B. S. Dewitt (Paris: Gordon and Breach), 343
Owen, F. N., Eilek, J. A., & Kassim, N. E. 2000, ApJ, 543, 611
Perlman, E. S., Adams, S. C., Cara, M., et al. 2011, ApJ, 743, 119
Perlman, E. S., Biretta, J. A., Sparks, W. B., Macchetto, F. D., & Leahy, J. P. 2001, ApJ, 551, 206
Rafferty, D. A., McNamara, B. R., Nulsen, P. E. J., & Wise, M. W. 2006, ApJ, 652, 216
Rees, M. J. 1984, ARA&A, 22, 471
Reynolds, C. S., Fabian, A. C., Celotti, A., & Rees, M. J. 1996, MNRAS, 283, 873
Sądowski, A., Narayan, R., Penna, R., & Zhu, Y. 2013, MNRAS, 436, 3856
Sérsic, J. L. 1968, Atlas de Galaxias Australes (Cordoba: Observatorio Astronomico)
Sparks, W. B., Macchetto, F., & Biretta, J. A. 1996, ApJ, 473, 254
Spruit, H. C., Stehle, R., & Papaloizou, J. C. B. 1995, MNRAS, 275, 1223
Stawarz, Ł., Aharonian, F., Kataoka, J., et al. 2006, MNRAS, 370, 981
Stiavelli, M., Peletier, R. F., & Carollo, C. M. 1997, MNRAS, 285, 181
Tchekhovskoy, A. 2015, in Astrophysics and Space Science Library, Vol. 414, ed. I. Contopoulos, D. Gabuzda, & N. Kylafis, 45
Tchekhovskoy, A., Narayan, R., & McKinney, J. C. 2011, MNRAS, 418, L79
Tchekhovskoy, A., Narayan, R., & McKinney, J. C. 2010, ApJ, 711, 50
Walsh, J. L., Barth, A. J., Ho, L. C., & Sarzi, M. 2013, ApJ, 770, 86
Young, P. J., Westphal, J. A., Kristian, J., Wilson, C. P., & Landauer, F. P. 1978, ApJ, 221, 721
Young, A. J., Wilson, A. S., & Mundell, C. G. 2002, ApJ, 579, 560
Yuan, F., & Narayan, R. 2014, ARA&A, 52, 529